https://doi.org/10.5194/nhess-2020-63
Preprint. Discussion started: 16 March 2020

Natural Hazards and Earth System Sciences
Discussions

The assessment of earthquake-triggered landslides susceptibility with considering coseismic ground deformation

Yu Zhao[1, 2], Zeng Huang[1], Zhenlei Wei[1*], Jun Zheng[1], Kazuo Konagai[3]

1. College of Civil Engineering and Architecture, Zhejiang University, Hangzhou 310058, China
2. MOE Key Laboratory of Soft Soils and Geoenvironmental Engineering, Zhejiang University, Hangzhou 310058, China
3. International consortium on landslides, Kyoto 611-0011, Japan

* Contact author: Zhenlei Wei, email: weizhenlei@zju.edu.cn

Abstract

The distance to the surface rupture zone has been commonly regarded as an important influencing factor in the evaluation of earthquake-triggered landslides susceptibility. However, the obvious surface rupture zones usually do not occur in some buried-fault earthquakes cases, which mean lacking of the information about the distance to the surface rupture. In this study, a new influencing factor named coseismic ground deformation was added to remedy this shortcoming. The Mid-Niigata prefecture earthquake was regareded as the study case. In order to select a more suitable model for generating the landslides susceptibility map, three commonly used models named Logistic Regression (LR), Artificial Neural Networks (ANN) and Support Vector Machines (SVM) were also conducted to assess the landslides susceptibility. The performances of these three models were evaluated with the receiver operating characteristic (ROC) curve. The calculated results showed the ANN model has the highest AUC (area under the curve) value of 0.82. As the earthquake triggered more landslides in the epicenter area, which makes it more prone to landslides in further earthquakes, the landslides susceptibility in the epicenter area was also further evaluated.

Keywords: Earthquake triggered landslides; Landslide susceptibility mapping; coseismic ground deformation;

1. Introduction

Earthquake-triggered landslides are commonly seen in the earthquake disaster chain. The landslides not only bring loss of life and property but also seriously affect the post-earthquake rescue. By summarizing the data of 40 historical earthquakes events in the world, Keefer discovered that the earthquake-triggered landslide was the main reason for the loss of life and property (Keefer, 1984). More than 60 people were killed and nearly 100,000 people were displaced due to the Mid-Niigata earthquake in 2004 (Bandara and Ohtsuka, 2017). In 2008, the Wenchuan earthquake triggered nearly 200,000 landslides, killing about 20,000 people (Xu et al., 2012b). At present, numerous researchers regarded the susceptibility mapping as an effective way to hazard mitigation and disaster management, and a number of models have been used to generate landslide susceptibility maps.

At present, one type of commonly used methods to evaluate the susceptibility of landslides is the physical-based method. For this type of method, the study area is

https://doi.org/10.5194/nhess-2020-63
Preprint. Discussion started: 16 March 2020

Natural Hazards and Earth System Sciences
Open Access
EGU
Discussions

usually divided into slopes units and then LEM or FEM are applied to calculate the safety factor (FS) of each slope unit (Saade et al., 2016). However, the physical mechanism of the landslide is often very complicated, especially for the landslides caused by earthquakes. Due to the difficulty of obtaining enough parameters for slope dynamic analysis, it still is a tough job to assess the landslide susceptibility with physical-based models in large-scale areas.

The statistical learning method was the another important method for landslide susceptibility assessment. This type of method is based on the assumption that future landslides would be easily to occur under similar conditions to those of the previous landslides. By analyzing the characteristics of the current landslides, a set of influencing factors are usually selected to implement statistical learning and evaluate the landslide susceptibility map (Pham et al., 2017; Ali et al., 2019; Lin et al., 2019). At present, many statistical learning methods have been used successfully to calculate the landslides susceptibility index (LSI) and generate the earthquake-triggered landslide susceptibility maps (Hong et al., 2017; Pham et al., 2016; Xu et al., 2012a; Yi et al., 2019). For example, Yang et al., (2015) established the susceptibility map of seismic landslides for the Lushan earthquake in Sichuan Province with an artificial weighting method. Shrestha and Kang (2019) used a maximum entropy model to produc the landslide susceptibility map of the central region of the Nepal Himalaya. However, the relatively good performance of these methods highly relies on the local geo-environment factors and self-features of the methods. For different study areas, the most accurate method is also different. Thus, it is necessary to make comparisons between

https://doi.org/10.5194/nhess-2020-63
Preprint. Discussion started: 16 March 2020

Natural Hazards and Earth System Sciences
Open Access
Discussions

various methods for selecting a more suitable method which produces a more reliable landslide susceptibility map (Bui et al., 2016).

Gorum et al. (2011) pointed out that the influencing factors of seismic landslide should include seismic correlation parameters, geology parameters, and topography parameters. Ding and Hu (2014) conducted the cluster analysis and the maximum possible classification method to study seismic landslides susceptibility of Beichuan County in the Wenchuan earthquake. Influencing factors contain land-use type, seismic intensity, and annual rainfall were selected to produce a reasonable susceptibility map. Since the earthquake-triggered landslides tend to occur frequently near the surface rupture zone (Xu et al., 2012b; Xu, 2014). Numerous scholars took the distance to the surface rupture zone as an influencing factor in the evaluation of landslides susceptibility (Xu et al., 2012b; Xu, 2014). However, it is worth noting that some buried- rupture earthquakes often do not have obvious surface rupture zones, the buried rupture earthquakes can also trigger abundant landslides (Xu, 2014). The evaluation accuracy of landslide susceptibility for buried rupture earthquake is affected by a lack of the factor of the distance to rupture (Regmi et al., 2016). Therefore, it is necessary to improve the accuracy of landslides susceptibility assessment for buried rupture earthquakes by introducing new influencing factors.

The Mid-Niigata Earthquake, which occurred in 2004, has become an important case for studying landslides due to good seismography and rich collection of seismic landslides. Wang et al., (2007) detected the relationship between landslide occurrence with geological, geomorphological conditions, slope geometry, and earthquake

https://doi.org/10.5194/nhess-2020-63
Preprint. Discussion started: 16 March 2020

parameters for the Mid-Niigata earthquake. Bandara and Ohtsuka (2017) used landslide occurrence ratio (LOR) to determine the correlation between the occurrence of earthquakes triggered landslides and geological attributes for the Mid-Niigata earthquake.

In this paper, based on GIS technology, three statistical methods and two different scales are evaluated to assess the landslides susceptibility caused by the Mid-Niigata earthquake. First of all, we selected lithology, elevation, slope, slope aspect, surface curvature, distance from the road and the peak value of earthquake acceleration as the influencing factors to evaluates the susceptibility of seismic landslides in the whole affected zone (large-scale area). For large-scale area, three different statistical learning methods (logical regression (LR), Support Vector Machine (SVM), and artificial neural network (ANN)) are utilized and compared to make reasonable seismic landslides susceptibility map. As the epicenter area that has higher landslide frequency more prone to earthquake-triggered landslides, the seismic landslides susceptibility in this area is further evaluated. Finally, given the fact of very short surface ruptures, the Mid-Niigata earthquake was regarded as a buried rupture earthquake (Maruyama et al., 2007). The coseismic ground deformation decomposed from high-resolution DEM is added as an influencing factor in order to improve the evaluation accuracy of the seismic landslide susceptibility for the epicenter area.

2. Study area

The Mid-Niigata earthquake occurred on October 23, 2004, The Japan Meteorological

Agency (JMA) measured the magnitude of the mainshock is 6.8, the epicenter is located at 37°18'16. 56"N, 138°50'10. 32"E, the focal depth is about 13.1 km (Chigira and Yagi, 2006; Kokusho et al., 2011). Within three days after the mainshock, more than 900 landslides were induced by the earthquake(Chigira and Yagi, 2006；Kokusho et al., 2014). After the earthquake sequences, a very small surface rupture was found along a previously unmapped northern extension fault zone. The length of the surface rupture was about 1 km (Maruyama et al., 2007). The surface slip of the Mid-Niigata earthquake event was also very small (< 20 cm of vertical displacement). In addition, the surface rupture zone is also far away from the epicenter zone, where the seismic landslides have concentrated distribution (Sato et al., 2005), i.e., the study area of seismic landslides susceptibility did not contain the surface rupture zone. So in this study, we consider the surface rupture zone has little effect on the formation of seismic landslides and regard the earthquake as a buried-rupture earthquake.

3. Datasets collection

3.1 landslide inventory

In this study, the assessment of seismic landslides susceptibility is performed on two scales, the large area, and the epicenter area. As shown in Fig. 1, the large-scale area is 22 km wide (east to west), and 40 km long (north to south). The total area of the large-scale area is about 880 km2. The epicenter area is 7 km long (north to south), and 9 km wide (west to east). The total area is about 56 km2. The epicenter area is located in the bordering area between Nagaoka City and Ojiya City.

https://doi.org/10.5194/nhess-2020-63
Preprint. Discussion started: 16 March 2020

Natural Hazards and Earth System Sciences
Discussions

Many methods have been utilized to set up landslide inventory maps, including satellite image interpretation, aerial photography, field survey and historical landslide records (Vařilová et al., 2015). In this research, the landslide inventory map was interpreted from satellite image data and then checked by field survey data (Kokusho et al., 2009; Kokusho 2008). As shown in Figure 1a, a totally of 957 landslides locations were recorded in the large-scale area, most of which are distributed in the mountainous area around the epicenter area and spread to the northeastern mountainous area. There are also some landslides located in the eastern and southern mountain areas. The landslides inventory map of the epicenter area is also shown in Fig. 1b.

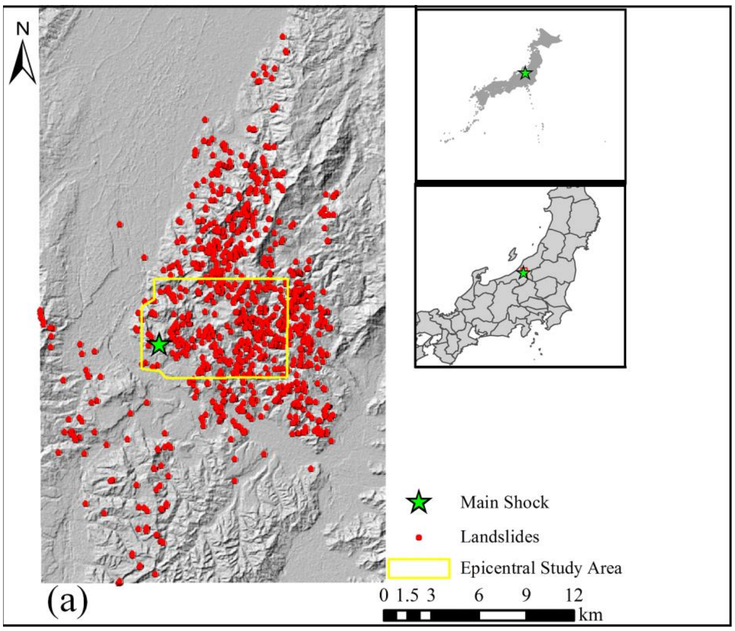

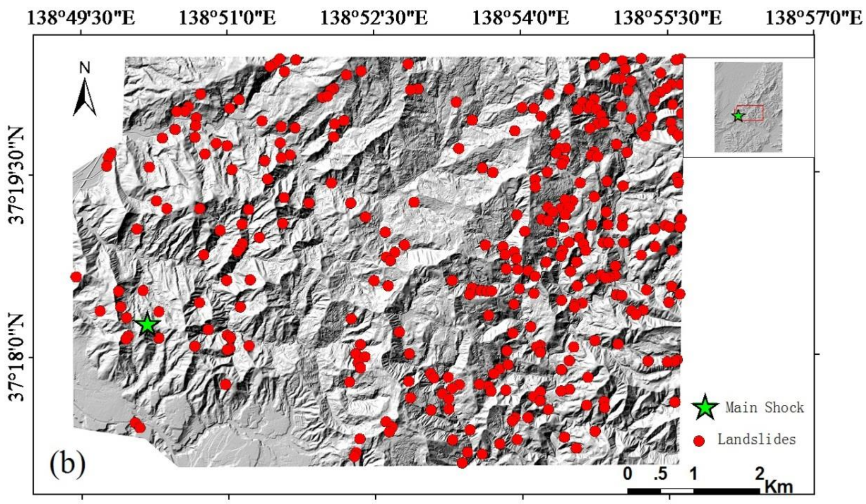

Fig.1 Locations of landslides in the study area (a) Large- scale area (b) epicenter area

3.2 Landslide influencing factors

The factors that affected the occurrence of earthquake-triggered landslide usually include geology, topography, hydrology, climate, human activities, earthquake-related parameters and etc. Based on the availability of data and impacted factors used in previous studies (Reichenbach et al., 2018), seven landslide factors influencing (lithology, elevation, slope, slope aspect, surface curvature, peak ground acceleration and the distance from the road) are take into consideration for landslide susceptibility analysis for the large-scale area. In the later analysis in the epicenter area, coseismic ground deformation was added as an influencing factor.

Lithology directly determines the physical and mechanical properties of the slope, which have a direct impact on slope stability. The lithology data used in this paper is redrawn from the 1: 50000 geological map of Nagaoka and Ojiya by the Geological

https://doi.org/10.5194/nhess-2020-63
Preprint. Discussion started: 16 March 2020

Natural Hazards and Earth System Sciences
Open Access
Discussions

Survey of Japan's Ministry of International Trade and Industry. There are ten different lithology groups in the large-scale area (Table 1) and eleven different lithology groups in the epicenter area (Table 2). The lithology maps in the large-area and epicenter area are shown in Fig. 2a and Fig. 3a.

Table 1 Lithological distribution in the large-scale area.

Category	Lithology
S	Gonglomerate with mudstone
G	Gonglomerate with sandstone
SM	Sandstone with silt
M	Sandstone with mudstone
Vs	Volcanic rock
Ms	Mudstone
Shs	Shale
A	Residual soil
Ss	Sandstone
Gs	Gonglomerate

Table 2 Lithological distribution in the epicenter area area.

Category	Lithology
QHd	Accumulation of Holocene
QPt	Accumulation of Pleistocene
QPl	Ancient landslide deposits of Pleistocene
QPu	Gonglomerate of Pleistocene
NPw	Gonglomerate of Pliocene
NPs	Sandy mudstone of Pliocene
NPu	Mudstone of Pliocene
NPk	Mudstone with sandstone of Pliocene
Nv	Volcanic rock of Pliocene
NMs	Shale of Miocene

The elevation also affects the occurrence of seismic landslides (Hasegawa et al., 2009). The elevation has bee regarded as a key factor determining gravitational potential

https://doi.org/10.5194/nhess-2020-63
Preprint. Discussion started: 16 March 2020

energy of terrain. The elevation data used in this paper is generated from the 30 m resolution DEM data obtained from ASTER Global Digital Elevation Model (ASTER GDEM). The elevations maps of the large-scale area and the epicenter area are shown in Fig. 2b and Fig. 3b, respectively.

The slope angle has a direct impact on slope stability that determines the ratio of anti-sliding force to sliding force. The slope angle in the study area ranges from 0° to 57.82° as shown in Fig.2c for the large-area. The Fig.3c shows the distribution of slope angle in epicenter area. The 0° slope angle means a flat area. The west part of the large-scale area is almost flat area, whereas the mountains mainly spread from NE direction to SW direction.

The influence of slope aspect on the stability of slope is multifaceted. Different slope directions have different influences of solar radiation and rainfall on the slopes that control the moisture of terrain that affects landslide occurrences. According to previous studies (Hong et al., 2017; Pham et al., 2016; Xu et al., 2012a), the slope aspect is divided into nine groups. The slope aspect maps of the large study area and the epicenter area are shown in Fig. 2d and Fig. 3d, respectively and the P and FL means the flat area..

Surface curvature determines the pooling and dispersion of surface water and affects the strength and stability of rocks and soils. In addition, there is a strong correlation between soil thickness and surface curvature due to soil sedimentation caused by the water flow. The surface curvature distributions in large-scale and epicenter area are shown in Fig. 2e and Fig. 3e, respectively.

The peak ground acceleration (PGA) of the earthquakes is the maximum absolute value

https://doi.org/10.5194/nhess-2020-63
Preprint. Discussion started: 16 March 2020

of the acceleration of the surface soil in an earthquake. Since the inertia forces generated by the earthquakes are important causes of the earthquake-triggered landslides, the PGA is generally chosen as the impact factor of landslides susceptibility. The distribution of peak accelerations in the large-scale area and the epicenter area is shown in Fig. 2f and Fig. 3f, respectively.

Human activities have also greatly impacted the topography features. Road construction not only produced a new steep cutting slope but also caused a great disturbance to the original slope. Therefore, the distance to the road is taken into account in the assessment of landslides susceptibility. In this study, the locations of high-grade roads like expressway were interpreted from the satellite image. The distances to road map were divided into seven classes (0–50, 50–100, 100–200, 200–300, 300–400, 400-500 and >500 m). The distances to road maps of the large-scale area and the epicenter area are shown in Fig. 2g and Fig. 3g, respectively.

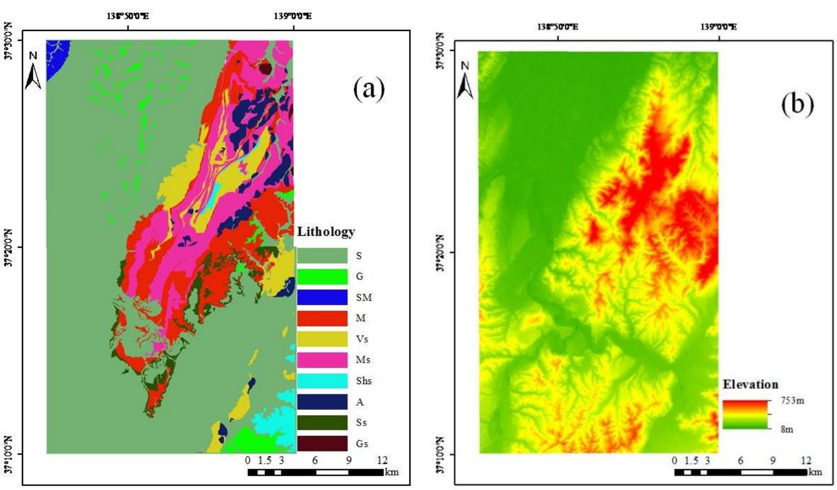

https://doi.org/10.5194/nhess-2020-63
Preprint. Discussion started: 16 March 2020

Natural Hazards and Earth System Sciences
Open Access
Discussions

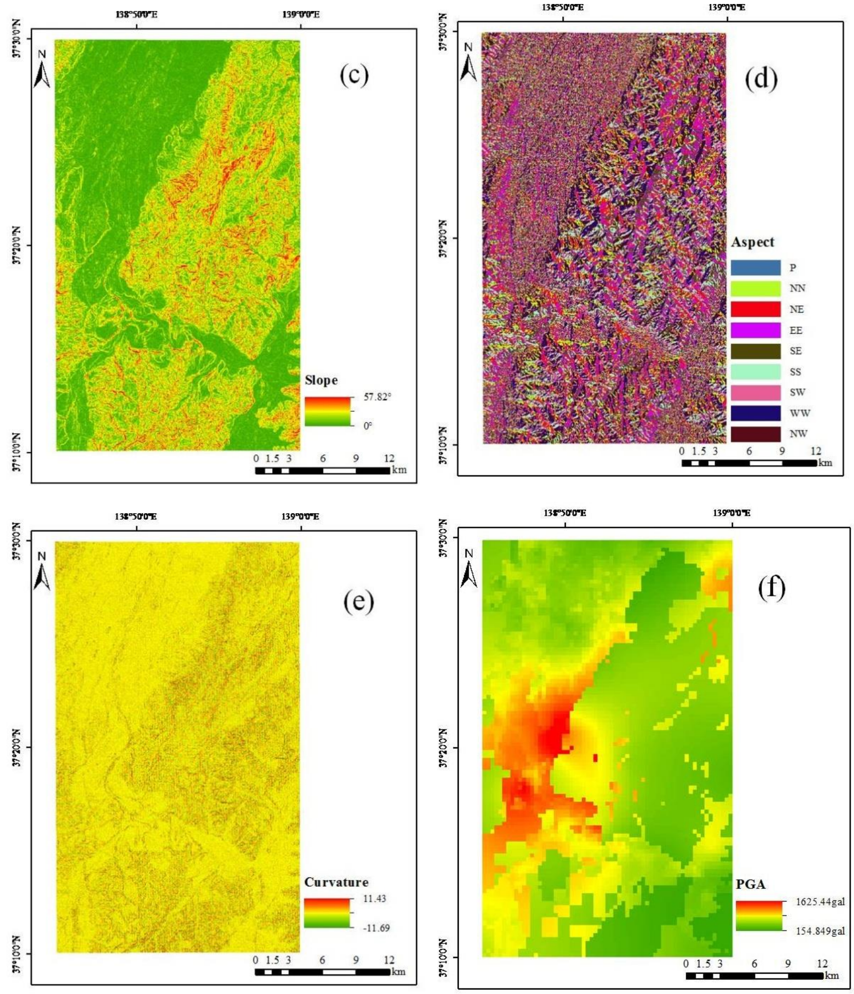

https://doi.org/10.5194/nhess-2020-63
Preprint. Discussion started: 16 March 2020

Natural Hazards and Earth System Sciences
Discussions

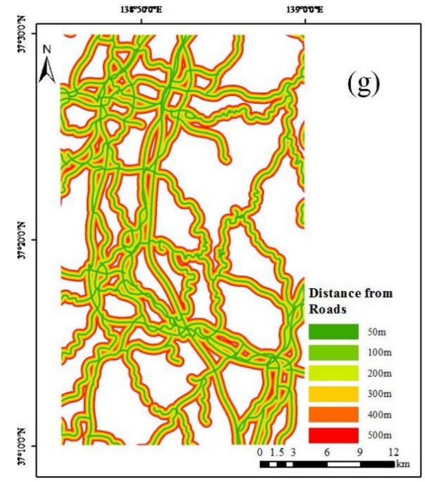

Fig.2 Landslide controlling factors of the large area, (a) lithology; (b) elevation; (c) slope degree; (d) aspect; (e) profile curvature; (f)PGA; (g) distance to roads

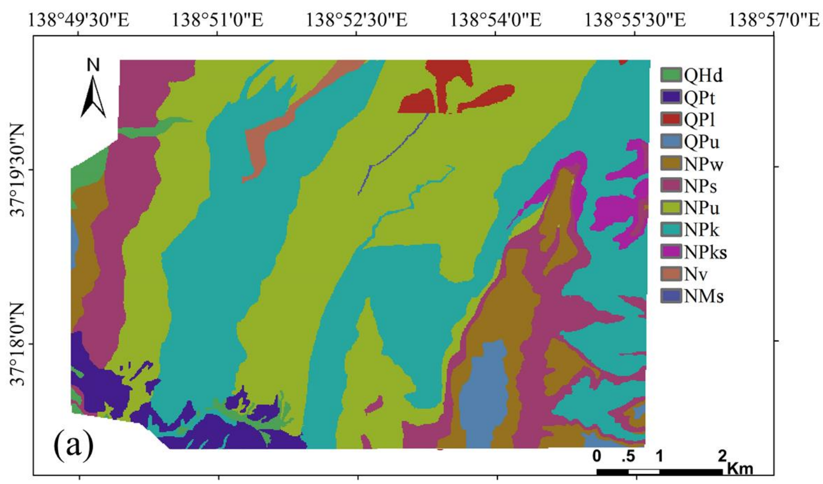

https://doi.org/10.5194/nhess-2020-63
Preprint. Discussion started: 16 March 2020

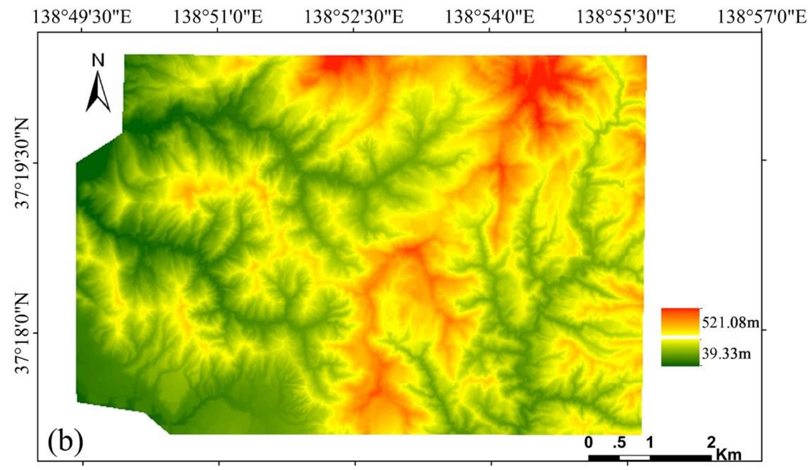

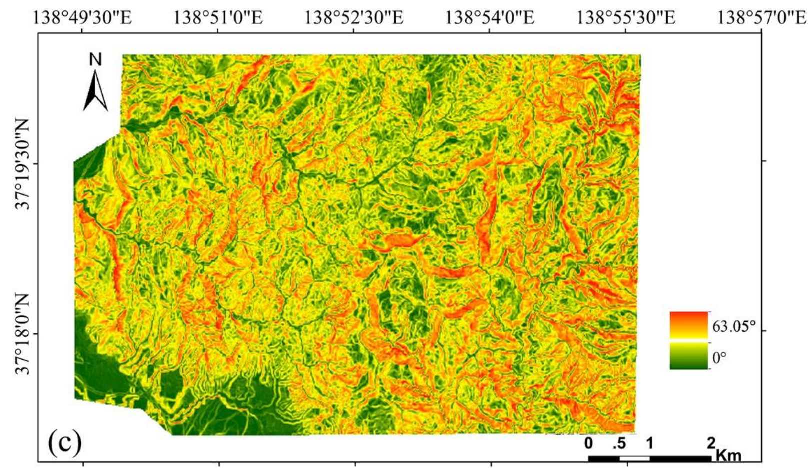

https://doi.org/10.5194/nhess-2020-63
Preprint. Discussion started: 16 March 2020

Natural Hazards and Earth System Sciences
Open Access
Discussions

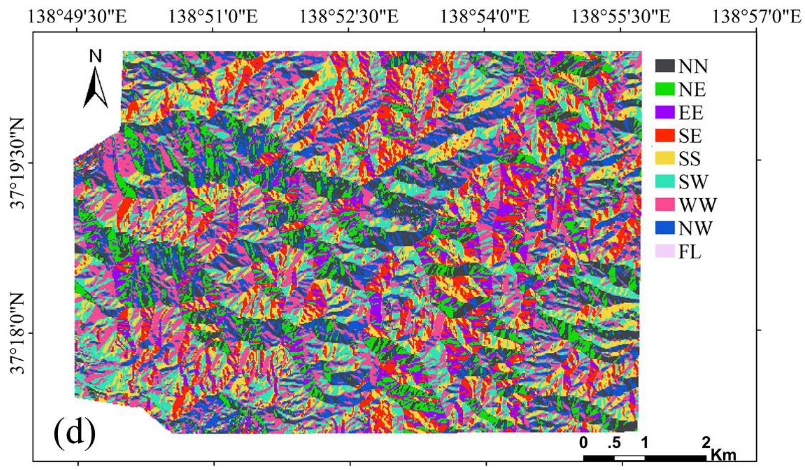

209

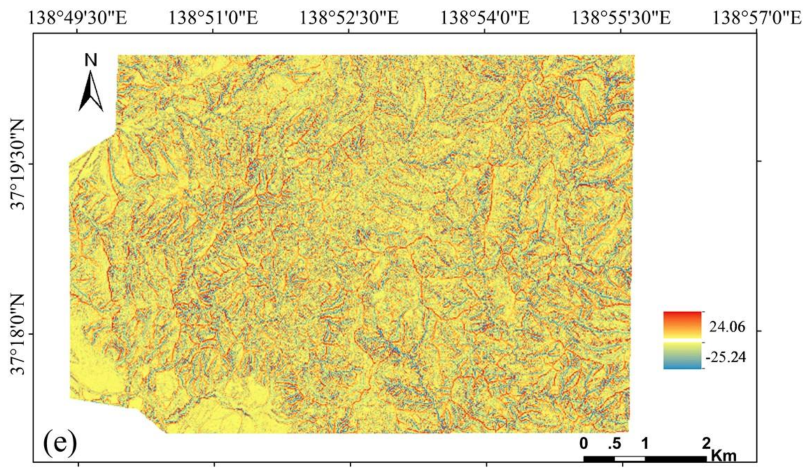

210

https://doi.org/10.5194/nhess-2020-63
Preprint. Discussion started: 16 March 2020

Natural Hazards and Earth System Sciences
Discussions

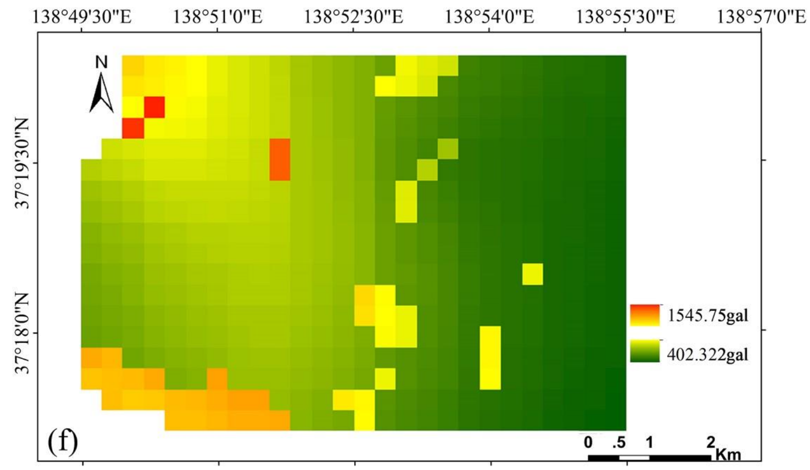

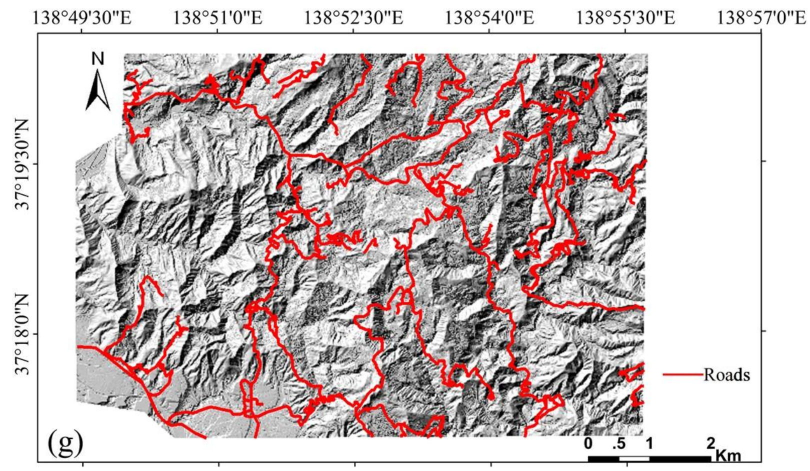

Fig. 3 Landslide controlling factors of the epicenter area, (a) lithology; (b) elevation; (c) slope degree; (d) aspect; (e) profile curvature; (f) PGA; (g) distance to roads

For the earthquakes with surface ruptures, the previous researches show that there is a clear connection between the landslide distribution and the distance to the rupture zone (Xu et., al 2012b; Xu, 2014), which means the distance to the surface rupture could be used as an influencing factor. However, for the buried-rupture earthquakes, as the very short or no surface rupture is exposed, it is difficult to establish the relationship between the distribution of landslides and surface rupture. Therefore, it is necessary to introduce new influencing factors to improve the accuracy of landslides susceptibility analysis for buried rupture earthquakes.

The coseismic ground deformation characterizes the absolute permanent ground deformation before and after the earthquake and it has been demonstrated tha there is a good correlation between landslides distribution and the values of coseismic ground deformation(Chang et al., 2005; Zhao et., al 2014). Therefore, the coseismic ground deformation could make up for the disadvantage of the losing surface rupture in the assessment of seismic landslide susceptibility to a certain extent. The coseismic ground deformation can be obtained by decomposed high-resolution DEM before and after the earthquake (Zhang et al., 2010; Zhao et al., 2014). Fig. 4 illustrates the description of landform changes in Lagrangian and Eulerian manners. Supposing that a small patch i of the ground surface with one particular node mapped on it is inclined in East-West (x) and North-South (y) directions, Δz_i^e is expressed in terms of the Lagrangian vector $\{\Delta x_i^l \ \Delta y_i^l \ \Delta z_i^l\}$ of the movement of the patch as:

$$\Delta z_i^e = \{t_{x,i} \quad t_{y,i} \quad 1\} \cdot \{\Delta x_i^l \quad \Delta y_i^l \quad \Delta z_i^l\}^T. \qquad (1)$$

where $t_{x,i}$ and $t_{y,i}$ are tangents of the patch plane in x and y directions, respectively. Taking three adjacent patches, i1, i2 and i3 in a triangle, and using the displacement of its center $\{\Delta x_i^l \ \Delta y_i^l \ \Delta z_i^l\}$ as the representative displacement vector of the triangle, the following simultaneous equations are to be satisfied

$$\begin{Bmatrix} \Delta z_{i1}^{e} \\ \Delta z_{i2}^{e} \\ \Delta z_{i2}^{e} \end{Bmatrix} = \begin{bmatrix} t_{x,i1} & t_{x,i1} & 1 \\ t_{x,i1} & t_{x,i1} & 1 \\ t_{x,i1} & t_{x,i1} & 1 \end{bmatrix} \begin{Bmatrix} \Delta x_{i}^{l} \\ \Delta x_{i}^{l} \\ \Delta x_{i}^{l} \end{Bmatrix} = T \bullet \begin{Bmatrix} \Delta x_{i}^{l} \\ \Delta x_{i}^{l} \\ \Delta x_{i}^{l} \end{Bmatrix}. \quad (2)$$

An assumption that the triangle undergoes a rigid body translation is used in the formulation above. The inclination of the moving plane (plane i1) is essential for calculating $t_{x,i}$ and $t_{y,i}$. Suppose the equation of the moving plane is expressed as:

$$z = ax + by + c \quad (3)$$

where a= $t_{x,,i1}$=tan$\theta_{x,,i1}$, b= $t_{y,i1}$=tan$\theta_{y,i1}$

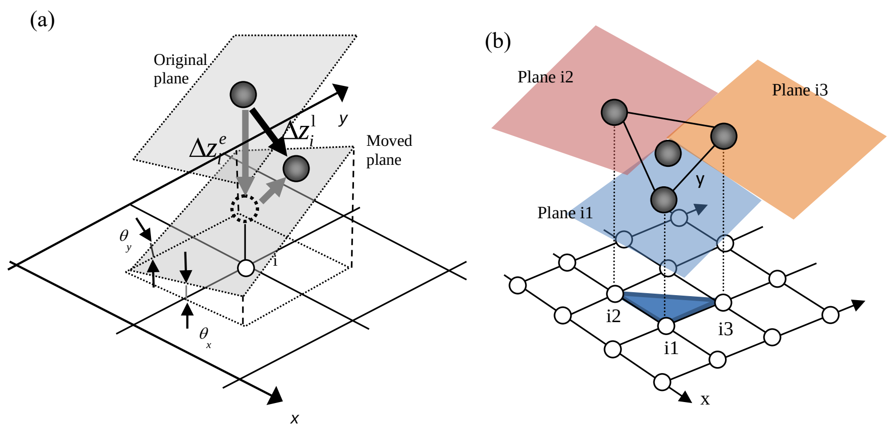

Fig.4 Description of landform change in the Lagrangian and Eurlaian manners, (a)scheme of one point (b) scheme of three-point

Zhao et al., (2012) provides a more rigorous solution method, including the definition of a nominal plane, the improvement of DEM comparability and matrix condition test. In this study, we used the method that is proposed by Zhao et al., (2012) to calculate the vacoseismic ground deformation. Note that the decomposition algorithm requires high resolution (2m) DEM. In this study, only the epicenter area was scanned via airborne LiDAR in 2003 and 2007, respectively. Thus, the coseismic ground deformation is added as an influencing factor for the epicenter area only. The

https://doi.org/10.5194/nhess-2020-63
Preprint. Discussion started: 16 March 2020

Natural Hazards and Earth System Sciences
Open Access
Discussions

distribution of coseismic ground deformation in the epicenter area is shown in Fig. 5.

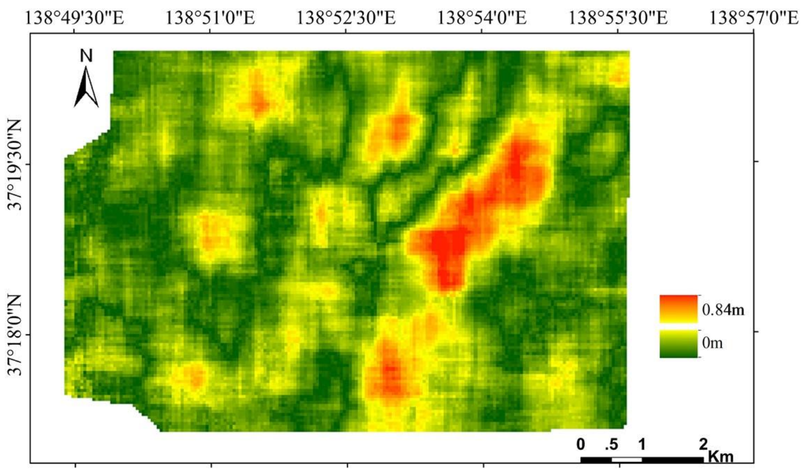

Fig. 5 The distribution of coseismic ground deformation in the epicenter area.

3.3 Landslides data preparation

In this study, the numbers of landslide points and non-landslide points are sampled at a ratio of 1:1.2 for the large-scale area. A total of 1117 non-landslide points data were randomly selected in the non-landslide area. Subsequently, 70% of the landslide points and non-landslide points were selected randomly from the landslide inventory map as the training dataset, with the rest as the testing dataset. In order to get optimum results, we randomly selected the sample points (landslides points and non-landslide points) for 10 times respectively. For different selection, the training and testing samples are different, but the numbers of sample points are the same. In the epicenter area, as the used the method to calculate the coseismic ground deformation needs high-resolution DEM, the whole epicenter areas were converted into 2 m pixels. The total number of

https://doi.org/10.5194/nhess-2020-63
Preprint. Discussion started: 16 March 2020

the pixels is 555324, and the number of seismic landslide pixels is 45852. Similarly, 70% of the landslide pixels and non-landslide pixels were selected randomly as the training dataset, with the rest 30% as the testing dataset.

4 Methodology

4.1 Logistic regression

Logistic regression is suitable for describing the relationship between categorical outcome (landslide or non-landslide) and input variables (landslide affecting factors). The principle of the LR is to analyze the spatial relationship between the landslides affecting factors and the occurrence of a landslide. The results of the regression usually can be interpreted as the probability which is constrained in the interval between 0 and 1.

The LR is indicated by an equation of the form:

$$Y = f(P) = \ln\left(\frac{P}{1-P}\right) = \beta_0 + \beta_1 X_1 + \beta_2 X_2 + \ldots + \beta_n X_n \quad (4)$$

where Y represents outcome variables (landslide or non-landslide), $X = X_1, X_2 \ldots Xn$ represents input variables, n is the n th landslide affecting factor, β_0 is the intercept condition, $\beta_1, \beta_2 \ldots \beta_n$ are the regression coefficients (Tu, 1996).

The SPSS 10.0 was used to conduct the LR analysis to predict the correlation between the occurrence of landslide and landslide affecting factors. The regression coefficients were then obtained.

The probability of a landslide event (P) can be determined from the following equation:

$$P = P(Y/X) = \frac{e^{\beta_0+\beta_1 X_1+\beta_2 X_2+\ldots+\beta_n X}}{1+e^{\beta_0+\beta_1 X_1+\beta_2 X_2+\ldots+\beta_n X}} \quad (5)$$

The probability values change from 0 to 1, with 0 indicating a 0% probability of landslide occurrences and 1 indicating a 100% probability.

4.2 Artificial neural networks (ANN)

ANN model has many advantages by comparing with other models (Yilmaz, 2009a). ANN could process the imprecise and fuzzy data without any assumptions. The ANN model with the most frequently used back-propagation BP algorithm (Pradhan and Lee, 2010b) is used in this paper.

The model mainly consists of one input layer, several hidden layers and an output layer. There are usually two stages for using ANN, the training stage and classifying stage. During the training stage, the hidden and the input layer neurons handle their inputs by a corresponding weight, sum the product, and then deal with the sum using a nonlinear transfer function to generate a result. During the classification period, the ANN predicts a target value by adjusting the weights in accordance with the errors between the actual output values and the target output ones and make the difference minimum.

In this study, the number of hidden layer nodes is calculated by Eq 6. (Yilmaz, 2009a).

$$N_h = 2N_i + 1 \quad (6)$$

Where N_i is the number of input nodes and N_h is the number of hidden nodes.

Then, a three-layer network with one input layer (7 neurons), one hidden layer (15 neurons) and one output layer was used in the large-scale area. In the epicenter area, a three-layer network consisting of one input layer (8 neurons), one hidden layer (17

https://doi.org/10.5194/nhess-2020-63
Preprint. Discussion started: 16 March 2020

neurons) and one output layer was utilized. It is important to decide the initial weight range as influencing the convergence of the model. In this study, the initial weights were randomly selected from a small range of [-0.25 to 0.25] as proposed by Yilmaz, (2009b).

4.3 Support vector machine (SVM)

The SVM model employs nonlinear transformations of the covariates into a higher dimensional feature space. The two main principles of SVM are the optimal classification hyperplane and the use of a kernel function. (Yao et al., 2008).

The detailed of a two-class SVM model is described as follows. Given a set of linear separable training vectors x_i (i=1,2…n) that consist of two categorical outcomes (landslide or non-landslide denoted as $y= \pm 1$), the purpose of the SVM is to find an n-dimensional hyperplane differentiating the two categories by the maximum gap.

Mathematically, the gap $\frac{1}{2}\|w\|^2$ could be minimized subject to the following constraints

$$y_i((w \cdot x_i)+b) \geq 1 \tag{7}$$

where $||w||$ is the norm of the normal of the hyperplane, b is a scalar base, and $(\cdot)$ denotes the scalar product operation. Using the Lagrangian multiplier, the cost function can be defined as:

$$L=\frac{1}{2}\|w\|^2-\sum_{i=1}^{n}\lambda_i(y_i((w \bullet x)+b)) \geq 1 \tag{8}$$

where λ_i is the Lagrangian multiplier. The solution can be obtained by the dual minimization of Eq. (8) with respect to w and b.

In this study, the two-class SVM method was used due to its good performance in landslide susceptibility analysis (Yao et al. 2008; Yilmaz 2010)

5. Model performance validation for large-scale area

5.1 Training and validating the statistical models

In this study, the performances of three models (LR, ANN and SVM) for the large-scale area were validated using receiver operating characteristic (ROC) curve. The area under the curve (AUC) indicates how good the statistical model is. It means the model has a perfect performance when the AUC value equals to 1. A higher AUC value indicates better performance of the statistical model.

Because each sample datasets are selected randomly, the landslides susceptibility calculated by the same model is not the same. In order to determine the best model, the models are utilized for ten times analyses of randomly selected datasets, respectively. For different analyses, the training and testing samples are different. For the same analyses, the training samples and testing samples are the same for all three models. The area under the ROC curve (AUC) of each analysis was compared to explore the difference of three methods. The results are shown in Table 3.

https://doi.org/10.5194/nhess-2020-63
Preprint. Discussion started: 16 March 2020

Table 3 The AUC value of different models in large-scale area

Number	1	2	3	4	5	6	7	8	9	10	Statistical value	
Model	%	%	%	%	%	%	%	%	%	%	Average value	Variance value
LR	82.0	81.6	82.3	80.2	81.4	80.2	81.4	80.7	81.6	82.0	81.3	0.49
ANN	83.3	82.4	83.6	81.3	82.1	82.0	82.1	82.3	82.8	83.1	82.5	0.44
SVM	80.8	80.9	81.8	80.1	80.7	79.4	80.4	80.5	80.5	81.8	80.7	0.47

Table 3 shown as the ANN model performed the best among the three models with the highest AUC value, and the accuracy of the SVM model was worst. Based on the maximum AUC values of ten simulations, the ANN simulation result was also the best (83.6%). The average value and variance of the ANN model were 82.5% and 0.44%, which was better than the LR and SVM models. It means the robustness of the ANN model is better than LR and SVM models.

Yilmaz (2009a) used three models including frequency ratio (FR), ANN and LR to generate the landslide susceptibility maps of Kat County (Tokat–Turkey). The result showed the ANN model performed better than other models. In Yilmaz (2010), four different models including conditional probability (CP), LR, ANN, and SVM models were utilized to assess the landslide susceptibility of Koyulhisar (Sivas, Turkey). The results also showed the performance of the ANN model was best. Some other research also showed the ANN model performed more accurate than other models (Yesilnacar and Topal 2005; Pradhan and Lee 2010c; Gómez and Kavalgu 2005). We consider the

ANN model performed better than the other models because it has a good global searching ability and can learn the near-optimum solution without the gradient information of error functions. As there about a total of 2000 samples in the calibration and validation set. Large numbers of samples in the calibration stage will lead to sufficient training of the model and establish an appropriate structure of ANN model. So the ANN model performs well on the condition those large numbers of samples were available. For any algorithm, the quantity and quality of samples have key impacts on the accuracy of the predicted results the algorithm makes.

5.2 Development of landslide susceptibility maps

In this study, all three models have been used to calculate the landslide susceptibility index (LSI) of each point, then generating the landslide susceptibility maps. There are several mathematical methods including quantiles, natural breaks, standard deviation, equal intervals, and descending area percentage to be reclassified the LSI (Ayalew et al., 2004). Among the above methods, the descending area percentage technique is the most widely used. In this study, the descending area percentage technique was used. The landslide susceptibility maps were constructed into four classes: low (40%), moderate (30%), high (20%), and very high (10%). The landslide density was used to assess the performance of landslide susceptibility maps. The landslide density (LD) is defined as the ratio of the numbers of landslide and the area of each susceptible class.

The calculated landslide densities by using the three different models are shown in Table 4. It can be observed that all maps present good spatial predictions of landslides

https://doi.org/10.5194/nhess-2020-63
Preprint. Discussion started: 16 March 2020

as landslide density is ascending from very low to very high class (Yilmaz, 2009b). The results using the ANN model show that the very high class contains 42.01% of the total landslides, however, it only covers 9.95% of the total study area and the LD of the very high class was 4.59. In comparison, the low classes only contain 3.34% landslides, however, it covers 40.15% area and the LD of the low class was 0.09. This indicates that the ANN model performed well in susceptibility classification as it fits well with the landslide inventories.

Table 4 The distribution of different classes area obtained by different methods

Model	Class	Area (km^2)	Times of landslides occurrence	Percentage of each susceptible class area (%)	Percentage of landslides in each susceptible class (%)	Landslides density （times/km^2）
LR	Very high	87.61	387	9.95	40.44	4.42
	high	175.55	350	19.95	36.57	1.99
	moderate	263.60	171	29.95	17.87	0.65
	low	353.35	49	40.15	5.12	0.14
SVM	Very high	87.71	473	9.97	49.43	5.39
	high	175.95	286	19.99	29.89	1.63
	moderate	264.16	126	30.01	13.17	0.48
	low	352.28	72	40.03	7.52	0.20
ANN	Very high	87.60	402	9.95	42.01	4.59
	high	175.54	352	19.95	36.78	2.01
	moderate	263.60	171	29.95	17.87	0.65
	low	353.37	32	40.15	3.34	0.09

The landslides susceptibility maps of different methods are shown as Fig. 6. The analyses result of LR, SVM and ANN models are very close. The epicenter area is a very high susceptible area, the northeast and the southwest mountain area are high and

https://doi.org/10.5194/nhess-2020-63
Preprint. Discussion started: 16 March 2020

very high susceptible areas respectively, and the northern plains area is basically distributed with low susceptible class. The susceptibility map of the ANN model shows the high susceptible areas and low susceptible areas are more concentrated into blocks, and zonation produced by the SVM and LR are more dispersed. Overall, all three models could generate reasonable landslides susceptibility maps.

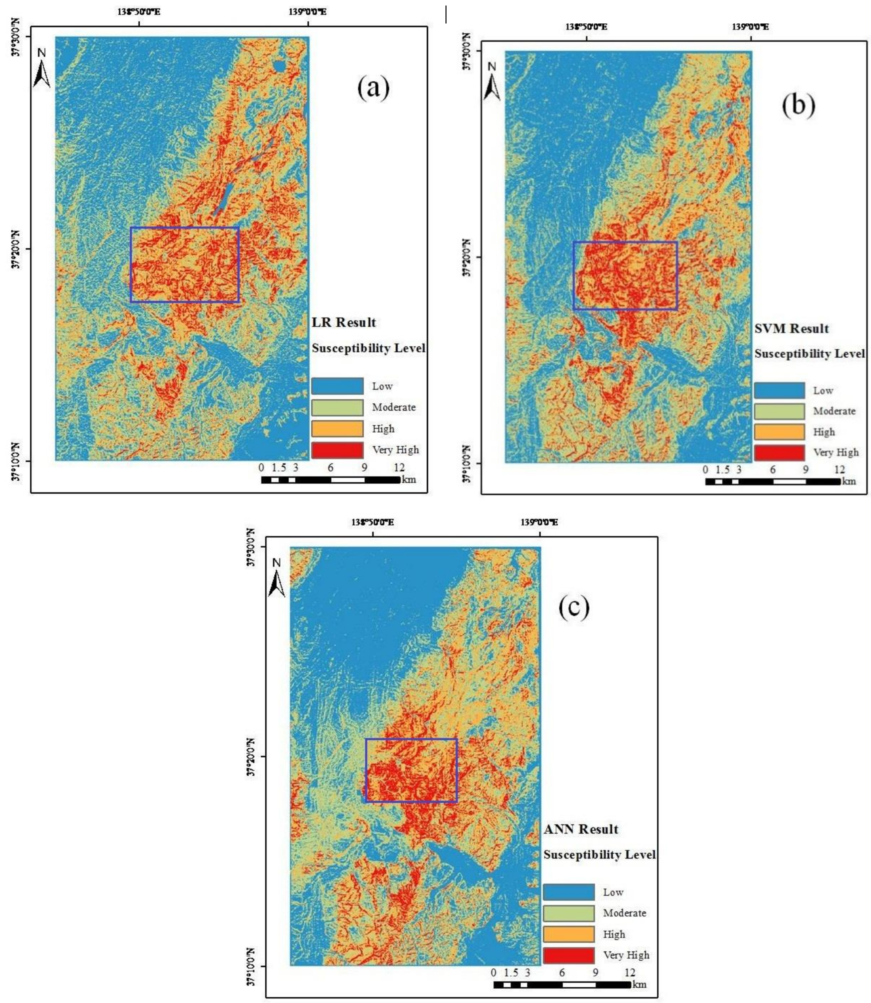

Fig. 6 Landslide susceptibility maps using different models for the large area. (a) LR model (b) SVM model (c) ANN model

https://doi.org/10.5194/nhess-2020-63
Preprint. Discussion started: 16 March 2020

6. Model performance validation for epicenter area

From the landslide susceptibility map of the large-scale area, it is known that the susceptibility level in the epicenter area is generally high. Since it is still too costly to remediate all slopes in the approximately 60 km^2 area, it is necessary to further evaluate the landslides susceptibility of the epicenter area. It can be seen in Section 5 that the ANN model is the most suitable model for landslides susceptibility assessment in this area. Therefore, we only use the ANN model to analyze and evaluate the landslides susceptibility in the epicenter area.

Firstly, in order to evaluate the significance of landslides susceptibility analysis with considering different scales. The values of AUC for the epicenter area are calculated in two different conditions. Firstly, we calculate the values of AUC based on the corresponding calculated LSI of the epicenter area from the large-scale (whole affected area) datasets. Then, the values of AUC are calculated based on the calculated LSI from the epicenter area datasets. The values of AUC of the two different conditions are shown as Fig. 7. The results show the AUC is 56.2% based on the calculated LSI from the large-scale datasets, on the contrast the AUC is 72.3% based on the calculated LSI from the epicenter area solely. The results show it is necessary to assess the landslides susceptibility under different scales.

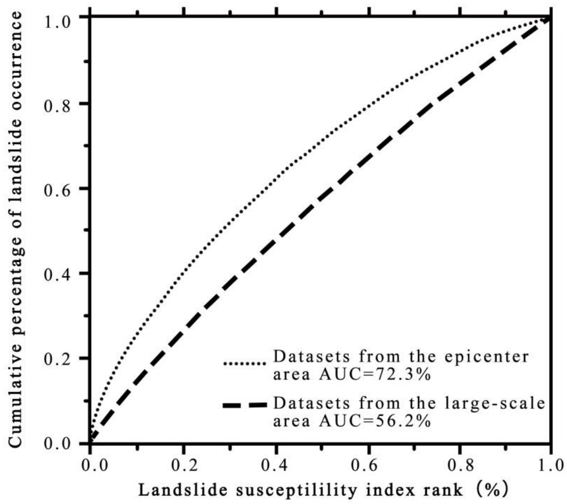

Fig.7 Analysis of the ROC curve under different scales

Then, in order to evaluate the effects of the new factor coseismic ground deformation on the assessment of landslides susceptibility, two different situations are considered. One situation regards the coseismic deformation as an influencing factor, whereas the other does not. Fig.8 shows the values of AUC with considering coseismic surface deformation or not. From Fig. 8, it could be known that the AUC is 72.3% without considering the coseismic surface deformation, on the contrast the AUC is 76.5% with considering the coseismic surface deformation. It means the coseismic surface deformation has a positive effect on the assessment of landslides susceptibility.

https://doi.org/10.5194/nhess-2020-63
Preprint. Discussion started: 16 March 2020

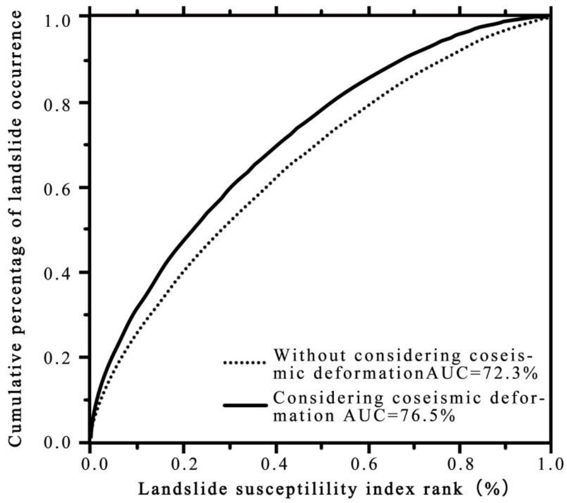

Fig.8 Analysis of the ROC curve with considering coseismic surface deformation or not

Influencing factors including lithology, elevation, slope, slope aspect, surface curvature, peak ground acceleration, the distance from the road and coseismic ground deformation were considered in the present study. Since the contribution of these factors to landslide models might be different, it is necessary to quantify the effects of influential factors on the assessment of landslides susceptibility. The Analysis of Variance method (ANOVA) has been utilized to evaluate the predictive capability of these factors. The factors with higher variance values indicate a higher contribution to landslide models and vice versa. The predictive capability of eight landslide affecting factors was shown in Table 5.

https://doi.org/10.5194/nhess-2020-63
Preprint. Discussion started: 16 March 2020

Table 5 the predictive importance of different influencing factors

Number	Influencing factor	Predictive importance
1	Lithology	0.213
2	Slope	0.207
3	PGA	0.169
4	Curvature	0.125
5	Coseismic ground deformation	0.093
6	Elevation	0.086
7	Slope aspect	0.057
8	Distance to roads	0.048

As Table 5 shown, lithology has the greatest impact on the occurrence of earthquake landslides and the impact of other factors is in order of slope, peak earthquake acceleration, curvature, coseismic ground deformation, elevation, aspect and distance from the road. The importance of coseismic surface deformation is higher than the elevation, aspect and distance from the road that are commonly chosen as influencing factors in the assessment of landslides susceptibility (Reichenbach et al., 2018). Although the earthquakes do not produce obvious ground rupture, the area with large coseismic surface deformation indicates that the movement of the rock mass may be further developed and the integrity of rock mass is reduced, which renders slopes prone to landslip in future earthquakes again. Therefore, especially in the case of buried fault earthquakes, coseismic surface deformation can be considered as an important influencing factor in the assessment of earthquake landslides susceptibility.

Subsequently, the landslides density and landslides susceptibility map of the epicenter area were obtained as shown in Table 6 and Fig 9. The results show that the very high class contains 40.44% of the total landslides, however, it only covers 8.6% of the

https://doi.org/10.5194/nhess-2020-63
Preprint. Discussion started: 16 March 2020

epicenter area and the LD of the very high class was 26.54. In comparison, the low classes contain only 5.12% landslides, however, it covers 40.15% area and the LD of the low class was only 0.73. The landslide density is increasing gradually between low class and very high class. This indicates that the landslide susceptibility map fits well with the landslide inventories.

Table 6 The distribution of different classes area in the epicenter area

	Class	Area (km^2)	Landslides occurrence	Percentage of each susceptible class area (%)	Percentage of landslides in each susceptible class (%)	Landslides density (times/km^2)
ANN	Very high	4.7853	127	8.6	40.44	26.54
	high	10.8605	115	19.51	36.57	10.57
	moderate	18.089	56	32.5	17.87	3.10
	low	21.9236	16	39.39	5.12	0.73

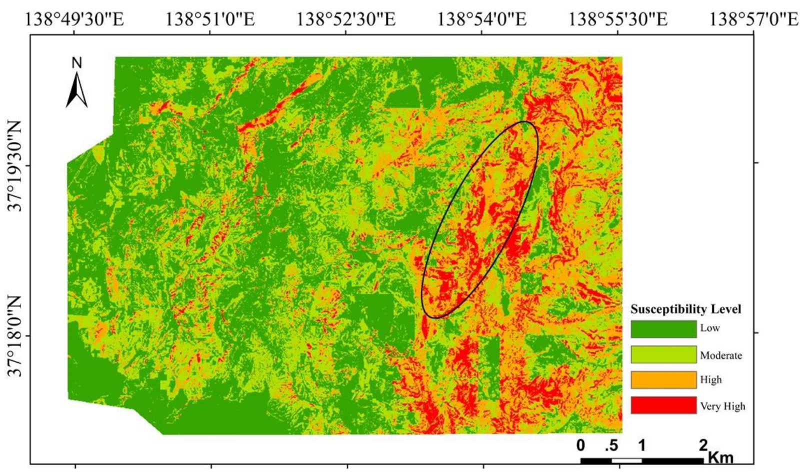

Fig. 9 Landslides susceptibility map of epicenter area

As shown in Figure 9, the very high-class area is mainly distributed along the long axis of the ellipse in the east of the study area, and a large amount of deep-seated landslide occurred in this area. The high susceptibility area is also distributed in the northwestern area. The occurrence possibility of landslides in the central area and southwest plain area is relatively low. Compared with the epicenter area parts in the landslides susceptibility map of large-scale, the landslides susceptibility maps obtained by the epicenter area research have a better discrimination degree, which can meet the key prevention and control requirements in the small area.

7. Conclusion

In this paper, the LR, ANN, and SVM models are applied to generate landslide susceptibility maps based on the 2004 Mid-Niigata earthquake-triggered landslide inventories. Seven impact factors, such as lithology, elevation, slope, aspect, surface curvature, peak acceleration and the distance from the road are selected as the influenced factors. The ROC curve evaluation results clearly demonstrate that the map obtained from the ANN model performed the best among the three models. The variance of AUC for randomly selected datasets by ANN is also the smallest, which means the ANN model has excellent robustness.

Therefore, the ANN model can be used for the assessment and the development of landslide susceptibility map. Then, the significance of landslides susceptibility analysis with considering different scales is also evaluated. The results show the AUC is 56.2% based on the datasets from the large-scale, on the contrast the AUC is 72.3% based on the datasets from the epicenter area solely. The results show it is necessary to assess the landslides susceptibility under different scales. At the same time, we included the coseismic ground deformation as the influencing factor for landslides susceptibility in

https://doi.org/10.5194/nhess-2020-63
Preprint. Discussion started: 16 March 2020

the epicenter area. The AUC increased from 0.723 to 0.765 after considering the newly added factor. Therefore, for the buried rupture earthquake, the coseismic surface deformation can be considered as an important factor to evaluate the susceptibility of landslides.

Acknowledgment

This research was supported financially by the Fundamental Research Funds for the Central Universities (2019FZJD002). We appreciate Prof. Fuchu Dai in Beijing University of Technology for his advice on improving the study.

Author contributions

ZY, ZH and ZW conceived this research. ZY, ZJ and KK designed the methodology and performed the experiments. ZY and ZW analysed the results and wrote the paper. All authors contributed to the preparation of this paper.

Competing interests.

The authors declare that they have no conflict of interest.

References

Ayalew, L., Yamagishi, H. and Ugawa, N., 2004. Landslide susceptibility mapping using GIS-based weighted linear combination, the case in Tsugawa area of Agano River, Niigata Prefecture, Japan. Landslides, 1(1): 73-81.

Ali, S., Biermanns, P., Haider, R. and Reicherter, K., 2019. Landslide susceptibility mapping by using a geographic information system (GIS) along the China–Pakistan Economic Corridor (KarakoramHighway), Pakistan. Natural Hazards and Earth System Science, 19, 999–1022.

https://doi.org/10.5194/nhess-2020-63
Preprint. Discussion started: 16 March 2020

Bandara, S. and Ohtsuka, S., 2017. Spatial distribution of landslides induced by the 2004 Mid-Niigata prefecture earthquake, Japan. Landslides 14(6): 1877-1886.

Bui, D.T., Nguyen, Q.P., Hoang, N.D. and Klempe, H., 2016. A novel fuzzy K -nearest neighbor inference model with differential evolution for spatial prediction of rainfall-induced shallow landslides in a tropical hilly area using GIS. Landslides, 14(1): 1-17.

Chang, K.J., Taboada, A. and Chan, Y.C., 2005. Geological and morphological study of the Jiufengershan landslide triggered by the Chi-Chi Taiwan earthquake. Geomorphology, 71(3): 293-309.

Chigira, M. and Yagi, H., 2006. Geological and geomorphological characteristics of landslides triggered by the 2004 Mid Niigta prefecture earthquake in Japan. Engineering Geology, 82(4): 202-221.

Ding, M. and Hu, K., 2014. Susceptibility mapping of landslides in Beichuan County using cluster and MLC methods. Natural Hazards, 70(1): 755-766.

Gorum, T., Fang, X.M., Westen, C.J.V., Huang, R.Q., Xu,Q., Tang, C. and Wang, G.H., 2011. Distribution pattern of earthquake-induced landslides triggered by the 12 May 2008 Wenchuan earthquake. Geomorphology, 133(3–4): 152-167.

Gómez, H. and Kavzoglu, T., 2005. Assessment of shallow landslide susceptibility using artificial neural networks in Jabonosa river basin, Venezuela. Engineering Geology, 78(1–2): 11-27.

Hasegawa, S., Dahal, R.K., Nishimura, T., Nonomura, A. and Yamanaka, M., 2009. DEM-Based Analysis of Earthquake-Induced Shallow Landslide Susceptibility. Geotechnical & Geological Engineering, 27(3): 419-430.

Hong, H., Liu, J.Z., Zhu, A.X., Shahabi, H., Pham, B.T., Chen, W., Pradhan, B. and Bui, D.T., 2017. A novel hybrid integration model using support vector machines and random subspace for weather-triggered landslide susceptibility assessment in the Wuning area (China). Environmental Earth Sciences, 76(19): 652.

Keefer, D.K., 1984. Landslides caused by earthquakes. Geological Society of America Bulletin, 95(4): 406.

Kokusho, T., Koyanagi, T. and Yamada, T., 2014. Energy approach to seismically induced slope failure and its application to case histories –Supplement. Engineering Geology, 181: 290–296.

Kokusho, T., Ishizawa, T. and Hara, T., 2009. Slope failures during the 2004 Niigataken Chetsu earthquake in Japan. Earthquake Geotechnical Case Histories for Performance-Based Design, Balkema, CRC Press, 47-70.

Kokusho, T., 2008. Report of the 2004 Niigataken Chuetsu Earthquake Slope disaster database. Chuo University, Tokyo (In Janpanese).

Kokusho, T., Ishizawa, T. and Koizumi, K., 2011. Energy approach to seismically induced slope failure and its application to case histories. Engineering Geology, 122, (1-2) :115-128.

Lin, L., Lin, Q.G. and Wang, Y., 2017. Landslide susceptibility mapping on a global scale using the method of logistic regression. Natural Hazards and Earth System Science, 17, 1411–1424.

Maruyama, T., Iemura, K., Azuma, T., Yoshioka, T., Sato, M. and Miyawaki, R., 2007. Paleoseismological evidence for non-characteristic behavior of surface rupture associated with the 2004 Mid-Niigata Prefecture earthquake, central Japan. Tectonophysics, 429(1): 45-60.

Pham, B.T., Bui, D.T., Prakash, I., Long, H.N. and Dholakia, M.B., 2017. A comparative study of sequential minimal optimization-based support vector machines, vote feature intervals, and logistic regression in landslide susceptibility assessment using GIS. Environmental Earth Sciences, 76(10): 371.

Pham, B.T., Pradhan, B., Tien Bui, D., Prakash, I. and Dholakia, M.B., 2016. A comparative study of different machine learning methods for landslide susceptibility assessment. Environmental Modelling & Software, 84: 240-250.

Pradhan, B. and Lee, S., 2010a. Landslide susceptibility assessment and factor effect analysis: backpropagation artificial neural networks and their comparison with frequency ratio and bivariate logistic regression modelling. Environmental Modelling & Software, 25(6): 747-759.

Pradhan, B. and Lee, S., 2010b. Regional landslide susceptibility analysis using back-propagation neural network model at Cameron Highland, Malaysia. Landslides, 7(1): 13-30.

Pradhan, B. and Saro, L., 2010c. Delineation of landslide hazard areas on Penang Island, Malaysia, by using frequency ratio, logistic regression, and artificial neural network models. Environmental Earth Sciences, 60(5): 1037-1054.

Reichenbach, P., Rossi, M., Malamud, D.B., Mihir, M. and Guzzetti, F., 2018. A review of statistically-based landslide susceptibility models. Earth-Scienc Reviews, 180: 60-91.

Regmi, A. D., Dhital, M. R., Zhang, J. Q., Su, L,J. and Chen, X. Q., 2016. Landslide susceptibility assessment of the region affected by the 25 April 2015 Gorkha earthquake of Nepal. Journal of

https://doi.org/10.5194/nhess-2020-63
Preprint. Discussion started: 16 March 2020

Mountain Science, 3(11):1941-1957.

Saade, A., Abou-Jaoude, G. and Wartman, J., 2016. Regional-scale co-seismic landslide assessment using limit equilibrium analysis. Engineering Geology, 204: 53-64.

Sato, H.P., Sekiguchi, T., Kojiroi, R., Suzuki, Y. and Iida, M., 2005. Overlaying landslides distribution on the earthquake source, geological and topographical data: the Mid Niigata prefecture earthquake in 2004, Japan. Landslides, 2(2): 143-152.

Shrestha, S. and Kang, T. S., 2019. Assessment of seismically-induced landslide susceptibility after the 2015 Gorkha earthquake, Nepal. Bulletin of Engineering Geology and the Environment, 78(3):1829-1842.

Tu, J.V., 1996. Advantages and disadvantages of using artificial neural networks versus logistic regression for predicting medical outcomes. Journal of Clinical Epidemiology, 49(11): 1225-31.

Vařilová, Z., Kropáček, J., Zvelebil, J., Šťastný, M. and Vilímek, V., 2015. Reactivation of mass movements in Dessie graben, the example of an active landslide area in the Ethiopian Highlands. Landslides, 12(5): 1-12.

Wang, H.B., Sassa, K. and Xu, W.Y., 2007. Analysis of a spatial distribution of landslides triggered by the 2004 Chuetsu earthquakes of Niigata Prefecture, Japan. Natural Hazards, 41(1): 43.

Xu, C., 2014. Do buried-rupture earthquakes trigger less landslides than surface-rupture earthquakes for reverse faults? Geomorphology, 216: 53-57.

Xu, C., Dai, F., Xu, X. and Yuan, H.L., 2012a. GIS-based support vector machine modeling of earthquake-triggered landslide susceptibility in the Jianjiang River watershed, China. Geomorphology, s 145–146(2): 70-80.

Xu, C., Xu, X., Dai, F. and Saraf, A.K., 2012b. Comparison of different models for susceptibility mapping of earthquake triggered landslides related with the 2008 Wenchuan earthquake in China. Computers & Geosciences, 46(3): 317-329.

Yang, Z.H., Lan, H.X., Gao, X., Li, L.P., Meng, Y.S. and Wu, Y.M., 2015. Urgent landslide susceptibility assessment in the 2013 Lushan earthquake-impacted area, Sichuan Province, China. Natural Hazards, 75(3): 2467-2487.

Yao, X., Tham, L.G. and Dai, F.C., 2008. Landslide susceptibility mapping based on Support Vector Machine: A case study on natural slopes of Hong Kong, China. Geomorphology, 101(4): 572-

582.

Yilmaz, I., 2009a. Landslide susceptibility mapping using frequency ratio, logistic regression, artificial neural networks and their comparison: a case study from Kat landslides (Tokat-Turkey). Computers & Geosciences, 35(6): 1125-1138.

Yilmaz, I., 2009b. A case study from Koyulhisar (Sivas-Turkey) for landslide susceptibility mapping by artificial neural networks. Bulletin of Engineering Geology and the Environment, 68(3): 297-306.

Yilmaz, I., 2010. Comparison of landslide susceptibility mapping methodologies for Koyulhisar, Turkey: conditional probability, logistic regression, artificial neural networks, and support vector machine. Environmental Earth Sciences, 61(4): 821-836.

Yi, Y.N., Zhang, Z.J., Zhang, W,C., Xu, Q., Deng, C. and Li, Q.L., 2019. GIS-based earthquake-triggered-landslide susceptibility mapping with an integrated weighted index model in Jiuzhaigou region of Sichuan Province, China. Natural Hazards and Earth System Science, 19, 1973–1988.

Yesilnacar, E. and Topal, T., 2005. Landslide susceptibility mapping: a comparison of logistic regression and neural networks methods in a medium scale study, Hendek region (Turkey). Engineering Geology, 79(3–4), 251-266.

Zhang, Y.S., Yao, X., Xiong, T.Y., Ma, Y.S., Hu, D.G., Yang, N. and Guo, C.B., 2010. Rapid identification and emergency investigation of surface ruptures and geohazards induced by the m_s 7.1 yushu earthquake. Acta Geologica Sinica(English Edition), 84(6): 1315-1327.

Zhao, Y., Konagai, K. and Fujita. T., 2012. Multi-scale Decomposition of Co-seismic Deformation from High Resolution DEMs: a Case Study of the 2004 Mid-Niigata Earthquake. Acta Geologica Sinica(English Edition), 86(4): 1013-1021.

Zhao, Y and Konagai, K., 2014. Evidence of a hidden landslide slip surface beneath a mountain hamlet. Environmental Earth Sciences, 71(10): 4615-4624.